# Three-Dimensional Encrypted Printing of Carbon Dots via Meniscus-Guided Microprinting

| | |
|---|---|
| Journal: | *Materials Lab* |
| Manuscript ID | MATLAB-2025-0007.R1 |
| Manuscript Type: | Original Article |
| Date Submitted by the Author: | 11-Jun-2025 |
| Complete List of Authors: | Park, Seobin; Ulsan National Institute of Science and Technology, Department of Mechanical Engineering<br>Seo, Sejeong; Sookmyung Women's University, Department of Chemical and Biological Engineering<br>Kim, Jae Eun; Ulsan National Institute of Science and Technology, Department of Mechanical Engineering<br>Park, Hyeonjin ; Sookmyung Women's University, Department of Chemical and Biological Engineering<br>Kwon, Woosung; Sookmyung Women's University, Department of Chemical and Biological Engineering; Sookmyung Women's University, Institute of Advanced Materials and Systems,<br>Jung, Im Doo; Ulsan National Institute of Science and Technology, Department of Mechanical Engineering; Ulsan National Institute of Science and Technology, Artificial Intelligence Graduate School |
| Keywords: | 3D printing, Carbon dots, fluorescence, information encryption, Meniscus-guided micro printing |
| Speciality: | Engineering, Nanomaterials, Photonic Materials |
| | |

Academic Press

# Manuscript Submission Template

- **Title page**

Three-Dimensional Encrypted Printing of Carbon Dots via Meniscus-Guided Microprinting

- **Author list**

Seobin Park[1,†], Sejeong Seo[3,†], Jae Eun Kim[1], Hyeonjin Park[3], Woosung Kwon[3,4*], Im Doo Jung[1,2*]

[1]Department of Mechanical Engineering, Ulsan National Institute of Science and Technology (UNIST), Ulju-gun, Ulsan, 44919, Republic of Korea

[2]Artificial Intelligence Graduate School, Ulsan National Institute of Science and Technology (UNIST), Ulju-gun, Ulsan, 44919, Republic of Korea

[3]Department of Chemical and Biological Engineering, Sookmyung Women's University, 100 Cheongpa-ro 47-gil, Yongsan-gu, Seoul, 04310, Republic of Korea

[4]Institute of Advanced Materials and Systems, Sookmyung Women's University, 100 Cheongpa- ro 47-gil, Yongsan-gu, Seoul, 04310, Republic of Korea

[†]These authors equally contributed to this work

*Corresponding authors: Woosung Kwon, Im Doo Jung

E-mail: wkwon@sookmyung.ac.kr, idjung.unist.ac.kr

Academic Press


## Abstract

Carbon dots (CDs) offer a promising alternative for optoelectronic applications, featuring multicolor emission, biocompatibility, and low-cost synthesis from abundant precursors. The integration of CDs into intricately designed structures via micro-scale three-dimensional (3D) printing holds great potential for enhancing their optical and mechanical functionalities. This study presents a novel micro-printing strategy for achieving CD fluorescence by utilizing a CD-filled polymer ink composed of CDs, hydroxypropyl cellulose, and N, N-dimethylformamide (DMF). The ink forms polymer composites with uniformly dispersed CDs through the rapid evaporation of DMF at the micro-meniscus. As a result, the printed structures exhibit stable fluorescence under 365 nm UV light and enable continuous stacking and encrypted patterning of various 3D architectures. The findings of this study are anticipated to contribute to the development of a versatile and scalable manufacturing approach for biocompatible, multicolor fluorescent 3D optoelectronic systems.



## Keywords

3D printing, Carbon dots, fluorescence, information encryption, Meniscus-guided micro printing

Academic Press

- **Main text**

## 1. Introduction

Optically luminescent materials such as fluorescent dyes [1, 2], perovskite [3, 4], quantum dots [5-8] have become the cornerstone of optoelectronic technologies, driving innovations in light-emitting diodes (LEDs) [9-12], information encryption [6, 13-15], biomedical imaging [16, 17], flexible electronics [18], and actuators [19]. The convergence of functional nanomaterials with three-dimensional (3D) printing enables unprecedented opportunities for the fabrication of customized advanced structures [1, 7, 20-22]. However, these materials typically require separate chemical synthesis processes for each emission wavelength, and concerns regarding toxicity and environmental sustainability have limited their applicability in consumer products and biomedical fields. In contrast, carbon dots (CDs) have emerged as promising alternatives due to their ability to exhibit multicolor emission from a single material via tunable energy levels [16, 23-26], abundant and low-cost raw material [27], excellent photostability [28, 29], and intrinsic biocompatibility [17, 30].

The nontoxic nature and intrinsic biocompatibility [31, 32] of CDs have further expanded their utility into diverse bio-related applications. Recent studies demonstrate the integration of CDs with hydrogels via 3D printing for advanced functionalities such as biomedical application [32, 33], and cell proliferation [31]. However, current research on CDs has predominantly focused on macroscopic applications such as bulk hydrogels [34] and films [35-37], leaving a critical gap in their integration with micro-scale 3D printing. The synergistic potential between CD-based fluorescence and microfabrication techniques remains largely unexplored, limiting their utilization in functional microdevices [38].

Recent advances in two-photon lithography [39] and meniscus-guided micro 3D printing [7, 8, 40-43] have enabled the fabrication of highly intricate microscale architectures with micro-scale resolution. Leveraging CDs in such microfabrication platforms allows for the direct construction of fluorescent microstructures with controllable geometries and emission profiles.

In this study, we developed a novel CD-filled polymer ink incorporating organic-solvent-soluble CDs, doped with oxygen and nitrogen (referred to as O-CDs and N-CDs, respectively), enabling fabrication of microscale 3D fluorescent structures via a

meniscus-guided micro-printing strategy. The ink formulation consists of CDs, hydroxypropyl cellulose (HPC), and N,N-dimethylformamide (DMF). Upon printing, rapid evaporation of DMF at the micro-meniscus facilitates the formation of polymeric architectures with uniformly dispersed CDs, exhibiting stable fluorescence under 365 nm UV illumination. We achieved continuous stacking of complex 3D geometries and direct patterning of encrypted features. Notably, vertically stacked micro-pixels enable information encryption that remains undetectable by conventional imaging systems, offering intrinsic optical security at the microscale.

## 2. Materials and methods

### *2.1. CD synthesis*

Benzyl alcohol (anhydrous, 99.8%) and toluene-$d_8$ were purchased from Sigma-Aldrich. Urea (>99.0%) was purchased from Tokyo Chemical Industry Co., Ltd. Toluene (99.5%), ethanol (95%), n-hexane (95%) and citric acid (anhydrous, 99.5%) were purchased from Samchun Pure Chemicals. All the solutions were prepared using toluene, and all the chemicals were used without further purification. To synthesize CDs, different precursor combinations were used: 4221 mg of citric acid for O-CDs and 2110.5 mg of citric acid and 659.8 mg of urea for N-CDs. Each set of precursors was dissolved in 15 mL of benzyl alcohol and vigorously stirred under ambient conditions for 24 h. The resulting mixtures were then transferred to a stainless-steel hydrothermal autoclave and heated to 300 ℃ for approximately 9 h. To purify the synthesized CDs, ethanol and hexane were added to the reaction mixture, followed by ultrasonication to promote dispersion of the nanoparticles. The solution was then centrifuged at 8000 rpm for 15 min to remove larger agglomerates and unreacted precursors. This washing and centrifugation process was repeated three times to ensure high purity of the CDs. The final colloidal solution was dried in a vacuum oven at 60 ℃ for 24 h to yield a dry CD powder.

### *2.2. Preparation of fluorescence CD ink*

The inks were prepared by dissolving 0.005 g of CD powder in 10 mL of DMF (Sigma-Aldrich) ($C_{CD}$ = 0.5 mg ml$^{-1}$). To adjust the ink viscosity and control spreading behavior and shrinkage during printing, HPC (Sigma-Aldrich) was added to 2 mL of the CD-DMF solution, yielding inks with five different HPC concentrations ($C_{HPC}$ = 2.5, 5, and 10 mg mL$^{-1}$) based on a prediluted CD-DMF solution. The dissolution process was accelerated using a vortex mixer (MaXshake VM30; DAIHAN) for 5

minutes to ensure homogeneous mixing, followed by 20 minutes of sonication to enhance dispersion.

### *2.3. Preparation of micro-nozzles*

The glass pipettes were fabricated using a programmed heat-pulling process (P-97 Micropipette Puller, Sutter Instrument). The inner diameters of pipettes tip were set to 1, 2, 5, and 10 μm by adjusting the pulling parameters for each target size. Only pipettes with high-quality nozzle tips and no visible cracks or chipped edges were selected to ensure consistency and prevent contamination. The diameter of each pipette was measured using a standard optical microscope (T690C-PL; AmScope) immediately after fabrication and prior to printing.

### *2.4 Meniscus-guided micro printing process*

The printing was performed under ambient conditions of approximately 22 ℃ and 40% relative humidity. The ink-filled micro-nozzle approached the glass substrate. After contacting the substrate, the nozzle was moved 500 nm to the +Z direction to form a meniscus. Subsequently, the bed platform was precisely controlled along the predefined G-code path. The optimal printing parameters were defined as an ink with an HPC concentration ($C_{HPC}$) of 5 mg ml$^{-1}$, inner diameter of micro-nozzle of 5 μm, and a printing speed ($v_p$) of 1 μm s$^{-1}$. with 3-axis stepper motor stages (XA-05, ZA-05; Kohzu Precision) using a custom Python-based program. Finally, the nozzle was lifted in the +Z direction at the designated threshold speed for termination ($v_t$ = 2 mm s$^{-1}$) to complete the printing process. The side-view of the printing process was monitored in real-time using optical microscope system with X50 objective (Mitutoyo) and CMOS color camera (BFS-U3-51S5C-C, Blackfly).

### *2.5 Characterizations*

Transmission electron microscopy (TEM) was conducted using an HT7800 instrument (HITACHI). Dynamic light scattering (DLS) measurements were carried out with a Horiba SZ-100 particle size analyzer. Raman spectroscopy was performed using an Alvatek XperRam S spectrometer with a 532 nm laser excitation source. X-ray diffraction (XRD) analysis was conducted on a D8 Advance diffractometer (TRIO/TWIN, Bruker) using Cu Kα radiation at 40 kV and 40 mA. X-ray photoelectron spectroscopy (XPS) measurements were obtained with a VG Scientific ESCALAB 250 spectrometer equipped with an Al Kα X-ray source (1486.6 eV). UV-visible absorption

(ABS) spectra were recorded using a Scinco S-3100 spectrophotometer. Photoluminescence (PL) spectra were collected with a Jasco FP-8500 fluorometer. All optical measurements were performed using 10 mm × 10 mm QS-grade quartz cuvettes (111-QS, Hellma Analytics). The fluorescence properties of the printed structures were observed by exposing the samples to 365 nm UV light and inspecting them using a standard optical microscope (AmScope T690C-PL). Rheological properties of the CD inks were analyzed using rheometer (Thermoelectron Haake MARS III-ORM Package). Ink viscosity was analyzed via a strain sweep ranging from 0 to 30 $s^{-1}$, while a stress sweep at a constant frequency of 1 Hz was used to examine the dependence of storage and loss moduli on shear stress. The morphology and energy dispersive spectroscopy (EDS) analysis was performed using a field emission scanning electron microscope (Quanta 200 FE-SEM). Samples were coated with a 10-20 nm thick platinum layer using a table-top sputter in order to prevent charge accumulation.

## 3. Results and discussion

### 3.1. Synthesis and characterizations of the CDs

The organic-solvent-soluble CDs were synthesized via solvothermal carbonization using citric acid alone for O-CDs and a combination of citric acid and urea for N-CDs, in the presence of benzyl alcohol. During the high-temperature synthesis, benzyl alcohol underwent oxidation to form highly oxidative derivatives (HODs), such as benzaldehyde and benzoic acid. These HODs participated in the carbonization process, introducing oxygen-related defect sites within the CD structure, which are known to play a crucial role in shaping the optical properties of the CDs. For N-CDs, the inclusion of urea as a nitrogen source introduced additional nitrogen-related defect states, further modifying their optical behavior. These nitrogen-induced defects are also recognized as key contributors to the photophysical properties of CDs. A detailed synthesis procedure is described in the Materials and Methods section.

The morphology and size distribution of the synthesized CDs were characterized by TEM, revealing quasi-spherical particles with relatively uniform shapes, regardless of the synthesis process (**Fig. 1a** and **b**). Both O-CDs and N-CDs exhibited well-dispersed nanoparticles without significant aggregation. The average particle diameters were typically in the range of 5-10 nm, with narrow size distributions, as confirmed by statistical analysis of TEM images. High-resolution TEM images further revealed lattice fringes with an interplanar spacing of approximately ~0.21 nm, corresponding

to the (100) plane of graphitic carbon, suggesting a partially crystalline carbon core structure (**Fig. 1c** and **d**). DLS analysis indicated that the average hydrodynamic diameters of the O-CDs and N-CDs were 5.9 nm and 11.1 nm, respectively (**Fig. 1e**). These values are larger than those obtained from TEM measurements, which is expected due to the nature of DLS detecting the hydrodynamic radius, including the surrounding solvation layer and surface-bound functional groups. This effect is particularly pronounced for N-CDs, which may carry more surface-bound nitrogen-containing groups (e.g., amines or amides) that enhance hydration and electrostatic interactions, thereby enlarging the hydrodynamic size relative to O-CDs. Raman spectra (**Fig. 1f**) showed characteristic signals of partially graphitic carbon, comprising a mixture of $sp^2$- and $sp^3$-hybridized domains. Both types of CDs exhibited two distinct peaks at ~1362.45 $cm^{-1}$ and ~1580.23 $cm^{-1}$, corresponding to the D and G bands, respectively. The calculated D/G intensity ratio for both samples was approximately 0.857, suggesting a turbostratic structure, i.e., polyaromatic domains randomly distributed within an amorphous carbon matrix. This polycrystalline nature was further confirmed by XRD analysis (**Fig. 1g**). A broad diffraction peak centered at $2\theta = 30°$ indicated a predominance of disordered graphitic (turbostratic) carbon structures. Additionally, a weak and broad diffraction band between $2\theta = 40\text{-}50°$ suggested the presence of localized graphitic regions. Based on these observations, we conclude that the CDs possess a highly oxidized carbon framework embedded with graphitic subdomains.

XPS was employed to investigate the chemical structure of the CDs. The C 1s spectra of all samples (**Fig. S1a** and **b**) exhibited a characteristic peak at 284.8 eV, corresponding to C–C/C=C bonds, indicative of the carbonization of citric acid. The O 1s spectra (**Fig. S1c** and **d**) revealed peaks at 532 eV and 533 eV, attributed to C−O and C=O bonds, respectively, which originate from oxygen-containing functional groups derived from the hydroxyl and carbonyl groups of citric acid and benzyl alcohol. In the N 1s spectrum of the O-CDs (**Fig. S1e**), no distinct nitrogen-related peak was detected, indicating the absence of nitrogen species. In contrast, the N-CDs (**Fig. S1f**) displayed two clear peaks around 401 eV in the N 1s spectrum, corresponding to pyrrolic/pyridinic nitrogen and C–$NH_2$ functionalities. These findings confirm the successful incorporation of nitrogen into the N-CD structure.

**Fig. 2a** shows the UV-vis absorption (ABS) spectra of the CDs. Both O-CDs and N-CDs exhibited a strong, sharp absorption peak in the deep UV region (~250 nm), which

can be attributed to the π→π* transition typically associated with conjugated C=C or C=O bonds in aromatic systems. In addition, a broad shoulder extending into the near-UV region (~300–350 nm) was more pronounced in N-CDs, suggesting enhanced n→π* transitions due to the incorporation of nitrogen-containing functional groups such as amines or imides.

The PL emission spectra (**Fig. 2b**) and contour maps (**Fig. 2c** and **d**) reveal a clear red shift in the emission peak of N-CDs (477 nm) compared to O-CDs (424 nm). This spectral shift indicates a reduction in band gap energy, which can be attributed to the formation of nitrogen-induced mid-gap states. Nitrogen doping introduces localized defect sites such as pyridinic or graphitic N, which facilitate additional nonradiative and radiative relaxation pathways. As a result, the N-CDs exhibit lower-energy emission due to recombination between these defect states and the conduction band. The broader and more excitation-dependent PL profile of N-CDs also supports the presence of a more heterogeneous distribution of emissive states compared to O-CDs.

### 3.2. Meniscus-guided printing strategies and fluorescent microstructures

The detailed procedure of the meniscus-guided printing process using the CD-filled polymeric ink is illustrated in **Fig. 3**. A glass micropipette (inner diameter ≈ 5 μm), mounted on a three-axis motorized stage, is filled with pico-liter volumes of the CD ink. Upon contact between the nozzle and the substrate, a micro-meniscus is formed where rapid solvent evaporation occurs. As the nozzle translates, the ink within the pipette is spontaneously drawn toward the meniscus interface via convective flow, continuously forming a solidified polymer line (**Fig. 3a**). CDs dispersed within the printed structure exhibit bright green fluorescence under 365 nm UV light. **Fig. 3b–d** showcase three representative printing strategies. In **Fig. 3b**, lateral movement of the nozzle along the substrate enables continuous line printing and subsequent layer-by-layer stacking. To terminate printing, the nozzle is rapidly withdrawn above the threshold speed ($v_t$) required to disrupt the meniscus and detach cleanly from the pattern. In **Fig. 3c**, vertical translation of the nozzle at a speed below the meniscus collapse threshold allows for the fabrication of vertically aligned micro-pillars. Moreover, as shown in **Fig. 3d**, precise control of the nozzle below the $v_t$ facilitates the creation of arch-shaped interconnects, overcoming conventional limitations in printing overhang structures. All printed architectures exhibit uniform fluorescence under 365 nm UV light (**Fig. 3e–g**).

### 3.3. Fluorescence characteristics of CD inks

The ink used for printing was fabricated by dispersing CD powder in DMF, followed by the addition of HPC as a binder to achieve an optimal viscosity for stable meniscus formation. As shown in **Fig. 4a**, the CD ink exhibits fluorescence under only UV illumination, while no emission is observed under daylight. Using each ink, vertically aligned micro-pillar arrays were printed to form the letters "O" and "N", all displaying similar green–cyan emission profiles under UV light (**Fig. 4b-c**). This apparent color similarity arises from the broad emission spectra of the CDs, which span a wide visible range, thereby masking subtle differences in their emission maxima. When plotted on the CIE 1931 color diagram, the three emission colors appear closely clustered, indicating spectrally similar fluorescence characteristics (**Fig. 4d**). To evaluate the long-term stability of the printed CD-based structures, fluorescence retention tests were performed over a period of 60 days under ambient conditions. As shown in **Fig. S3**, both O-CD and N-CD - filled printed lines maintained their fluorescence intensity without noticeable degradation when stored at room temperature. Fluorescence images captured under UV illumination (365 nm) on Day 0 and Day 60 confirmed that the printed features preserved their luminescence and structural integrity over time. These results indicate that the CD-based inks possess excellent photostability and are suitable for applications requiring prolonged visibility or encryption stability in ambient environments.

### 3.4. Elemental distribution and rheological optimization of CD inks

EDS further confirmed the homogeneous distribution of carbon and oxygen which are key constituents of the CDs throughout the 3D printed structures (**Fig. 5a-b**). Ink viscosity plays a critical role in determining the fidelity of meniscus-guided printing. Insufficient viscosity can lead to spreading on the substrate, whereas excessive viscosity may result in pattern discontinuities or nozzle clogging, compromising the resolution and continuity of the printed features. The rheological behavior of HPC–DMF solutions with varying concentrations (2.5, 5, and 10 mg $ml^{-1}$) was investigated to evaluate their flow characteristics and viscoelastic properties. As shown in **Fig. 5c**, all samples exhibited a pronounced shear-thinning behavior, where viscosity decreased sharply with increasing shear rate, indicating pseudoplastic fluid characteristics. Notably, the viscosity values across the three concentrations converged in the high

shear rate region, suggesting that molecular alignment and flow-induced disentanglement of polymer chains dominate under elevated shear conditions. This behavior ensures that, under low printing speeds, the ink maintains sufficient viscosity to suppress undesired spreading and retain structural fidelity by sustaining a stable meniscus during deposition. Oscillatory shear measurements (**Fig. 5d**) further revealed that below the yield stress (~$10^2$ Pa), the storage modulus (G′) and loss modulus (G″) are nearly identical, indicating a balanced viscoelastic response. Once the applied shear stress exceeds the yield point, G′ drops below G″ (G′ < G″), facilitating ink flow without clogging the nozzle.

### 3.5. Printed microstructures

**Fig. 6** presents optical and SEM images of various microstructures fabricated via the three distinct meniscus-guided printing strategies**.** In **Fig. 6a**, a side-view optical image captures the continuous meniscus formation during a layer-by-layer deposition process, which enables vertical growth through successive stacking. The corresponding SEM image in **Fig. 6b** shows a well-defined multilayer structure, highlighting the uniform vertical stacking exhibiting a thickness of approximately 10 μm. **Fig. 6c** demonstrates the ability to form complex geometries by printing stacked alphabetic letters "CD", composed of ten layers with an individual layer thickness of approximately 500 nm. Finally, in **Fig. 6d**, a single-arch interconnect structure is shown, which was successfully fabricated overhanging structure without intermediate support.

### 3.6. Encrypted printing application of CD-infilled pillar structures

**Fig. 7** showcases a range of potential applications based on vertically printed pillar structures. When viewed from the top, individual pillars appear as bright fluorescent dots, enabling their use in graphical designs and information encryption. As shown in **Fig. 7a**, increasing the vertical dimension of the pillars leads to enhanced fluorescence intensity. Furthermore, reducing the inter-pillar spacing improves the spatial resolution of printed images. In **Fig. 7b**, we demonstrate the capability of achieving a minimum inter-pillar spacing of 10 μm using a 5 μm nozzle to fabricate pillars with a height of 20 μm. This corresponds to a theoretical resolution of up to 2540 pixels per inch (PPI). **Fig. 7c–e** show fluorescence and optical images of printed "Heart," "Fruit," and "Eiffel Tower" patterns, respectively. Building on this, an information encryption strategy was demonstrated using CD-filled and CD-free pure pillars (**Fig. 7f-g**). The word "UNIST" was printed using CD-filled pillars, while surrounding areas were filled with pillars

composed of pure ink, forming a 4 × 20 microarray. Under ambient white light, all pillars appear indistinguishable. However, upon exposure to 365 nm UV light, the hidden green-emissive text becomes clearly visible, highlighting the feasibility of fluorescence-based optical encryption.

## 4. Conclusion

This study presents a methodology for fabricating 3D microstructures with stable fluorescence characteristics by developing a CD-filled polymer ink and applying it to a meniscus-guided micro-3D printing technology. Printing with an $C_{HPC}$ of 5 mg ml$^{-1}$ at a $v_p$ of 1 μm s$^{-1}$ enabled the successful fabrication of a range of structures, not only simple structures such as lines, pillars, and overhangs, but also information encryption architectures. The printed structures exhibited uniform fluorescence under 365 nm UV light the need for any post-processing, attributed to the homogeneous dispersion of CDs within the printed body. This was further supported by EDS, which confirmed that the key elements of CDs, carbon and oxygen, were evenly distributed throughout the 3D structures. Furthermore, we demonstrated the potential of this platform for information encryption by fabricating a 4 × 20 microarray composed of alternating CD-filled and pure ink pillars. The tunable fluorescence of CDs under various conditions can offer additional advantages for developing advanced functional inks with multicolor emission and enhanced encryption capabilities. Overall, this work not only validates a robust method for micro-patterned information encryption but also highlights its promising applicability in diverse fields such as biomedicine and optoelectronics.

## 5. Acknowledgments

We gratefully acknowledge financial support from the Technology development Program (Grant No. S3248116) funded by the Ministry of SMEs and Startups (MSS, Korea), the National Research Foundation of Korea (NRF) grant funded by the Korea government (MSIT) (Nos. RS-2024-00416891, RS-2023-00211636, 2022R1A2C4002403), and the Institute of Information & Communications Technology Planning & Evaluation (IITP) grant funded by the Korea government (MSIT) (No. RS-2020-II201336, Artificial Intelligence Graduate School Program (UNIST)). This study contains the results obtained by using the equipment of UNIST Central Research Facilities (UCRF).

## 6. Conflict of interest

Academic Press

The authors declare no conflict of interest.

## 7. Author contributions

S. Park conducted the experiments, performed data analysis, and wrote the paper. S. Seo synthesized and characterized samples and wrote the paper. J. E. Kim and H. Park contributed to the experiments and manuscript preparation. W. Kwon and I. D. Jung conceived the original idea, supervised the project, and provided critical feedback on the manuscript. All authors discussed the results and contributed to the final version of the manuscript.

Academic Press

## 8.References

[1] F. Wang, Y. Chong, F. Wang, C. He, Journal of Applied Polymer Science 134(32) (2017) 44988.

[2] A.J. Ruiz, S. Garg, S.S. Streeter, M.K. Giallorenzi, E.P. LaRochelle, K.S. Samkoe, B.W. Pogue, Scientific Reports 11(1) (2021) 17135.

[3] A. Gao, J. Yan, Z. Wang, P. Liu, D. Wu, X. Tang, F. Fang, S. Ding, X. Li, J. Sun, Nanoscale 12(4) (2020) 2569-2577.

[4] H. Jeon, M. Wajahat, S. Park, J. Pyo, S.K. Seol, N. Kim, I. Jeon, I.D. Jung, Advanced Functional Materials 34(29) (2024) 2400594.

[5] H. Kim, S. Beack, S. Han, M. Shin, T. Lee, Y. Park, K.S. Kim, A.K. Yetisen, S.H. Yun, W. Kwon, Advanced Materials 30(10) (2018) 1701460.

[6] Y. Liu, F. Han, F. Li, Y. Zhao, M. Chen, Z. Xu, X. Zheng, H. Hu, J. Yao, T. Guo, Nature communications 10(1) (2019) 2409.

[7] J. Bae, S. Lee, J. Ahn, J.H. Kim, M. Wajahat, W.S. Chang, S.-Y. Yoon, J.T. Kim, S.K. Seol, J. Pyo, ACS nano 14(9) (2020) 10993-11001.

[8] J. Bae, S. Kim, J. Ahn, H.H. Sim, M. Wajahat, J.H. Kim, S.-Y. Yoon, J.T. Kim, S.K. Seol, J. Pyo, Advanced Engineering Materials 23(9) (2021) 2100339.

[9] J. Du, L. Sheng, Y. Xu, Q. Chen, C. Gu, M. Li, S.X.A. Zhang, Advanced Materials 33(20) (2021) 2008055.

[10] Y. Byun, D. Lee, S.W. Bae, S. Won, S. Cho, S.H. Lee, Y. Park, Y.-H. Kim, W. Kwon, Journal of Alloys and Compounds 991 (2024) 174435.

[11] D. Zhang, W. Xiao, C. Liu, X. Liu, J. Ren, B. Xu, J. Qiu, Nature Communications 11(1) (2020) 2805.

[12] P. Zhu, S. Thapa, H. Zhu, D. Venugopal, A. Sambou, Y. Yue, S.S. Dantuluri, S. Gangopadhyay, ACS Applied Electronic Materials 5(10) (2023) 5316-5324.

[13] Y. Liu, F. Li, L. Qiu, K. Yang, Q. Li, X. Zheng, H. Hu, T. Guo, C. Wu, T.W. Kim, ACS nano 13(2) (2019) 2042-2049.

[14] Y. Zhang, X. Le, Y. Jian, W. Lu, J. Zhang, T. Chen, Advanced Functional Materials 29(46) (2019) 1905514.

[15] W. Yao, Q. Tian, W. Wu, Advanced Optical Materials 7(6) (2019) 1801171.

[16] H. Kim, Y. Park, S. Beack, S. Han, D. Jung, H.J. Cha, W. Kwon, S.K. Hahn, Advanced science 4(11) (2017) 1700325.

[17] A. Dehghani, S.M. Ardekani, M. Hassan, V.G. Gomes, Carbon 131 (2018) 238-245.

[18] C. Lu, C. Wang, J. Yu, J. Wang, F. Chu, ChemSusChem 13(5) (2020) 893-902.

[19] Z. Li, P. Liu, X. Ji, J. Gong, Y. Hu, W. Wu, X. Wang, H.Q. Peng, R.T. Kwok, J.W. Lam, Advanced Materials 32(11) (2020) 1906493.

[20] Y. Xia, B. Xue, M. Qin, Y. Cao, Y. Li, W. Wang, Scientific Reports 7(1) (2017) 9691.

[21] Z. Zhang, N. Corrigan, A. Bagheri, J. Jin, C. Boyer, Angewandte Chemie International Edition 58(50) (2019) 17954-17963.

[22] Y. Ren, J. Feng, ACS Applied Materials & Interfaces 12(6) (2020) 6797-6805.

[23] Y. Park, J. Yoo, B. Lim, W. Kwon, S.-W. Rhee, Journal of Materials Chemistry A 4(30) (2016) 11582-11603.

[24] L. Rao, Q. Zhang, B. Sun, M. Wen, J. Zhang, G. Zhong, T. Fu, X. Niu, Nanomaterials 12(18) (2022) 3132.

[25] S. Park, S.H. Lee, Y. Kim, H. Park, G.-M. Kim, Y.-H. Kim, W. Kwon, Optical Materials 159 (2025) 116313.

[26] R. Sato, Y. Iso, T. Isobe, Langmuir 35(47) (2019) 15257-15266.

[27] T. Garcia-Millan, J. Ramos-Soriano, M. Ghirardello, X. Liu, C.M. Santi, J.-C. Eloi, N. Pridmore, R.L. Harniman, D.J. Morgan, S. Hughes, ACS Applied Materials & Interfaces 15(38) (2023) 44711-44721.

[28] S. Do, W. Kwon, Y.H. Kim, S.R. Kang, T. Lee, T.W. Lee, S.W. Rhee, Advanced Optical Materials 4(2) (2016) 276-284.

[29] L. Wang, W. Li, L. Yin, Y. Liu, H. Guo, J. Lai, Y. Han, G. Li, M. Li, J. Zhang, Science advances 6(40) (2020) eabb6772.

[30] K.K. Lee, N. Raja, H.-s. Yun, S.C. Lee, C.-S. Lee, Acta Biomaterialia 159 (2023) 382-393.

[31] X. Huang, M. Shi, H. Zhai, Y. Zhang, Y. Zhang, Y. Zhao, Polymer Chemistry 14(3) (2023) 268-276.

[32] P. Das, S. Ganguly, P.K. Marvi, M. Sherazee, X. Tang, S. Srinivasan, A.R. Rajabzadeh, Advanced Materials 36(48) (2024) 2409819.

[33] A. Khabibullin, M. Alizadehgiashi, N. Khuu, E. Prince, M. Tebbe, E. Kumacheva, Langmuir 33(43) (2017) 12344-12350.

[34] L. Qiao, M. Zhou, G. Shi, Z. Cui, X. Zhang, P. Fu, M. Liu, X. Qiao, Y. He, X. Pang, Journal of the American Chemical Society 144(22) (2022) 9817-9826.

[35] A. Segkos, I. Sakellis, N. Boukos, C. Drivas, S. Kennou, K. Kordatos, C. Tsamis, Nanoscale 12(18) (2020) 10254-10264.

[36] H.-A.S. Tohamy, Scientific Reports 15(1) (2025) 10337.

[37] M.O. Alas, G. Dogan, M.S. Yalcin, S. Ozdemir, R. Genc, ACS omega 7(34) (2022) 29967-29983.

[38] X.Y. Du, C.F. Wang, G. Wu, S. Chen, Angewandte Chemie International Edition 60(16) (2021) 8585-8595.

[39] A. Jaiswal, S. Rani, G.P. Singh, M. Hassan, A. Nasrin, V.G. Gomes, S. Saxena, S. Shukla, ACS nano 15(9) (2021) 14193-14206.

[40] J.H. Kim, S. Lee, M. Wajahat, H. Jeong, W.S. Chang, H.J. Jeong, J.-R. Yang, J.T. Kim, S.K. Seol, ACS nano 10(9) (2016) 8879-8887.

[41] Y. Liu, J. Yang, C. Tao, H. Lee, M. Chen, Z. Xu, H. Peng, X. Huan, J. Li, X. Cheng, ACS Applied Materials & Interfaces 14(5) (2022) 7184-7191.

[42] S. Hu, X. Huan, J. Yang, H. Cui, W. Gao, Y. Liu, S.F. Yu, H.C. Shum, J.T. Kim, Nano Letters 23(21) (2023) 9953-9962.

[43] J.H. Kim, S. Park, J. Ahn, J. Pyo, H. Kim, N. Kim, I.D. Jung, S.K. Seol, Advanced Science 10(3) (2023) 2205588.

Academic Press

- **Figures**

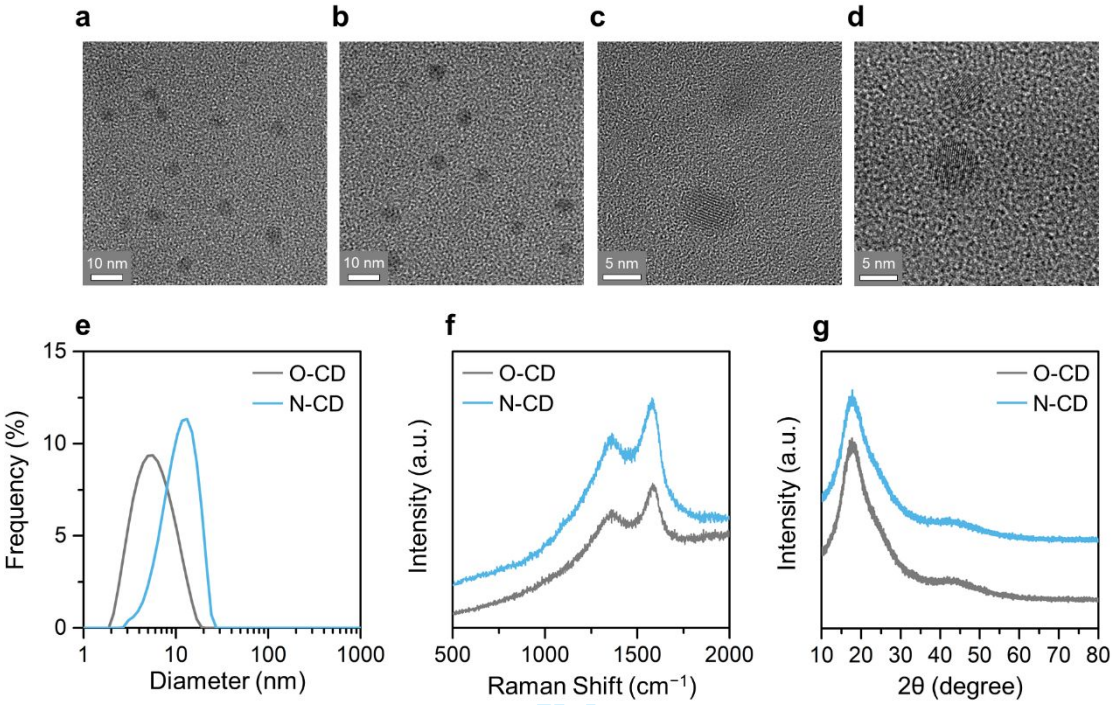


**Fig. 1.** Morphological characterizations of the CDs. TEM images of **a.** O-CD and **b.** N-CD. High-resolution TEM images of **c.** O-CD and **d.** N-CD. **e.** DLS size-distribution curves of the CDs. **f.** Raman spectra of the CDs. **g.** XRD patterns of the CDs.

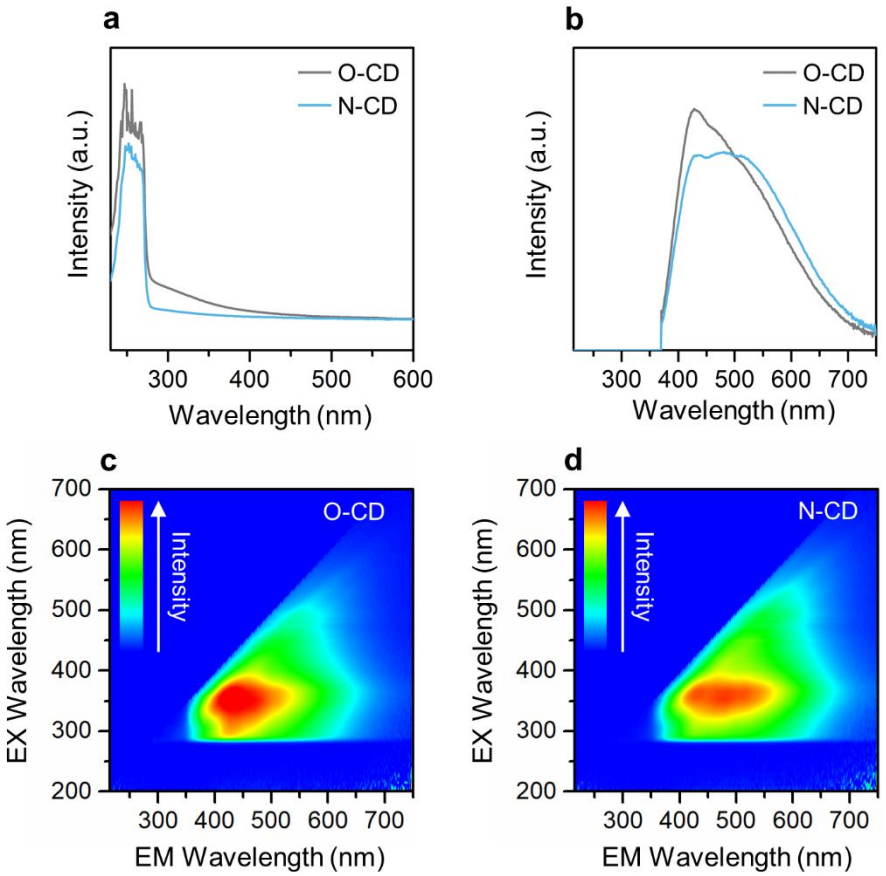


**Fig. 2.** Optical analyses of the CDs. **a.** ABS spectra of the CDs. **b.** PL emission spectra of the CDs. PL emission contour maps of **c.** O-CD and **d.** N-CD. EX and EM in the axis titles refer to excitation and emission, respectively.

Academic Press

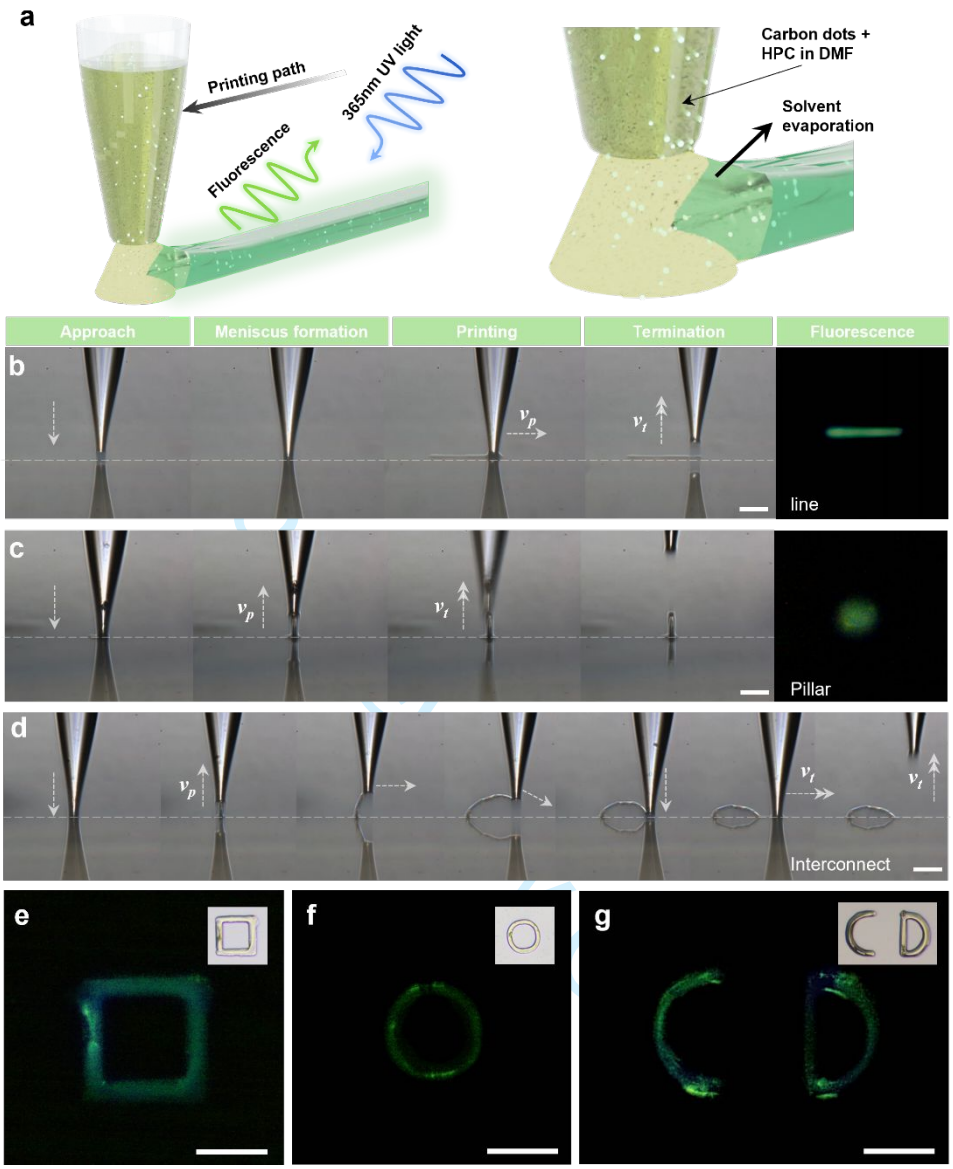


**Fig. 3.** Meniscus-guided micro printing of the CD-filled ink and printing techniques. **a.** Schematic of printing and fluorescence in printed patterns under UV light. **b-d.** Various printing techniques for printing of **b.** line, **c.** pillar, **d.** interconnect and their fluorescence images. **e-g.** Printing applications for writing a plane figures and alphabets using continuous layer-by-layer printing method.

Academic Press

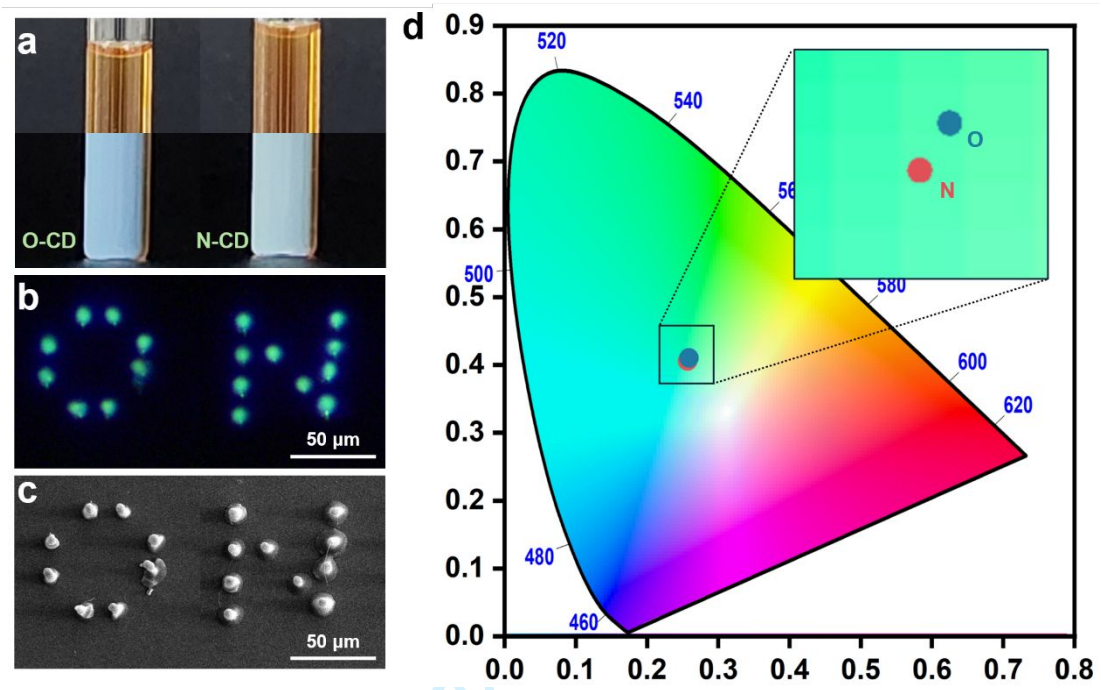


**Fig. 4. a.** Optical images of the O- and N-CD-filled inks under daylight and 365 nm UV light. **b.** Optical images of the printed CD ink and comparison of fluorescence colors of the pillars filled with O- and N-CD. **c.** SEM image of the letter "O" and "N". **d.** CIE chromaticity diagram of color coordinates of O- and N-CD fluorescence colors.

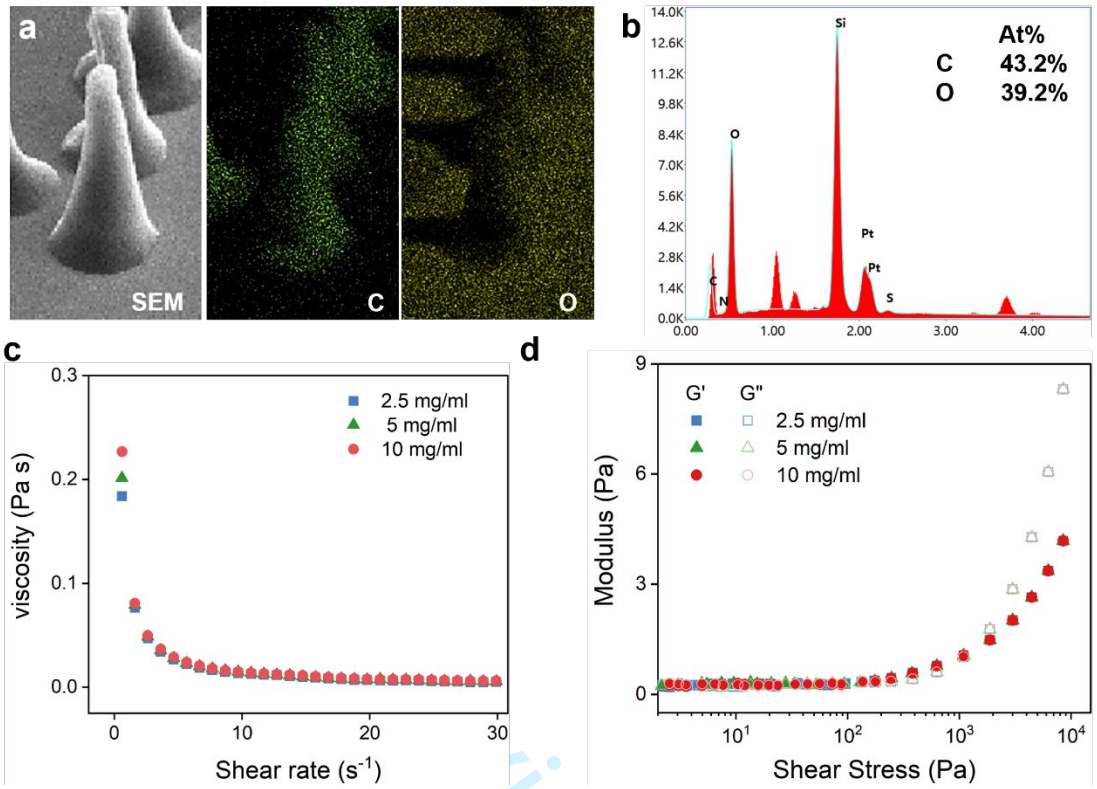


**Fig. 5. a.** EDS images of the elemental mapping in the printed structures. **b.** energy spectrum results of CD-HPC architectures. **c, d.** Rheological properties of CD-HPC inks with different HPC concentration.

Academic Press

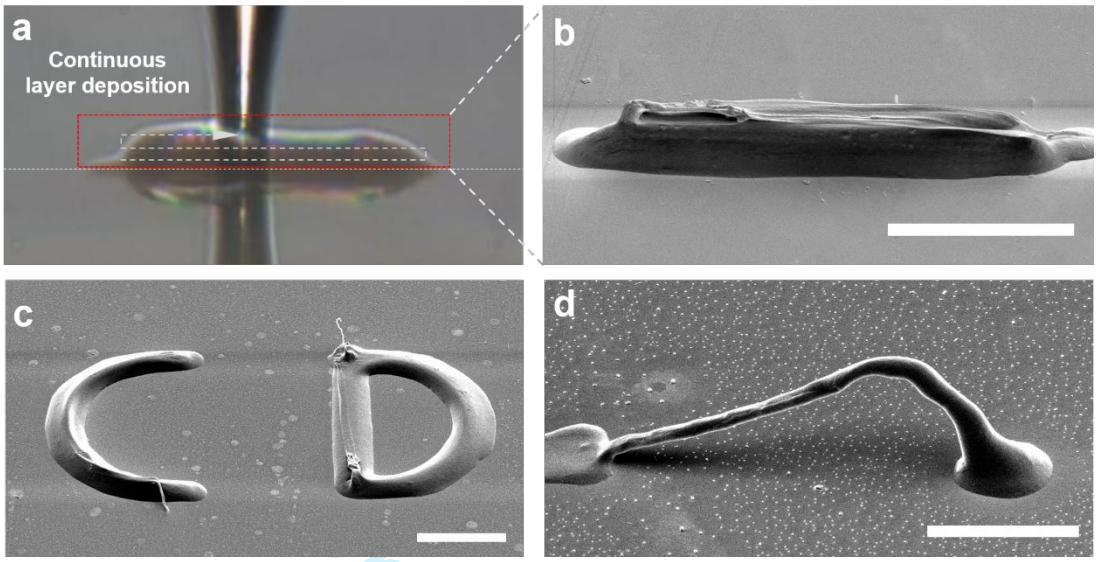


**Fig. 6.** Optical and SEM images of different printed structures**. a, b.** wall structure printed through continuous layer deposition, **c.** letter "CD" with multi-layer printing, **d.** Single-arch interconnect structure.

Academic Press

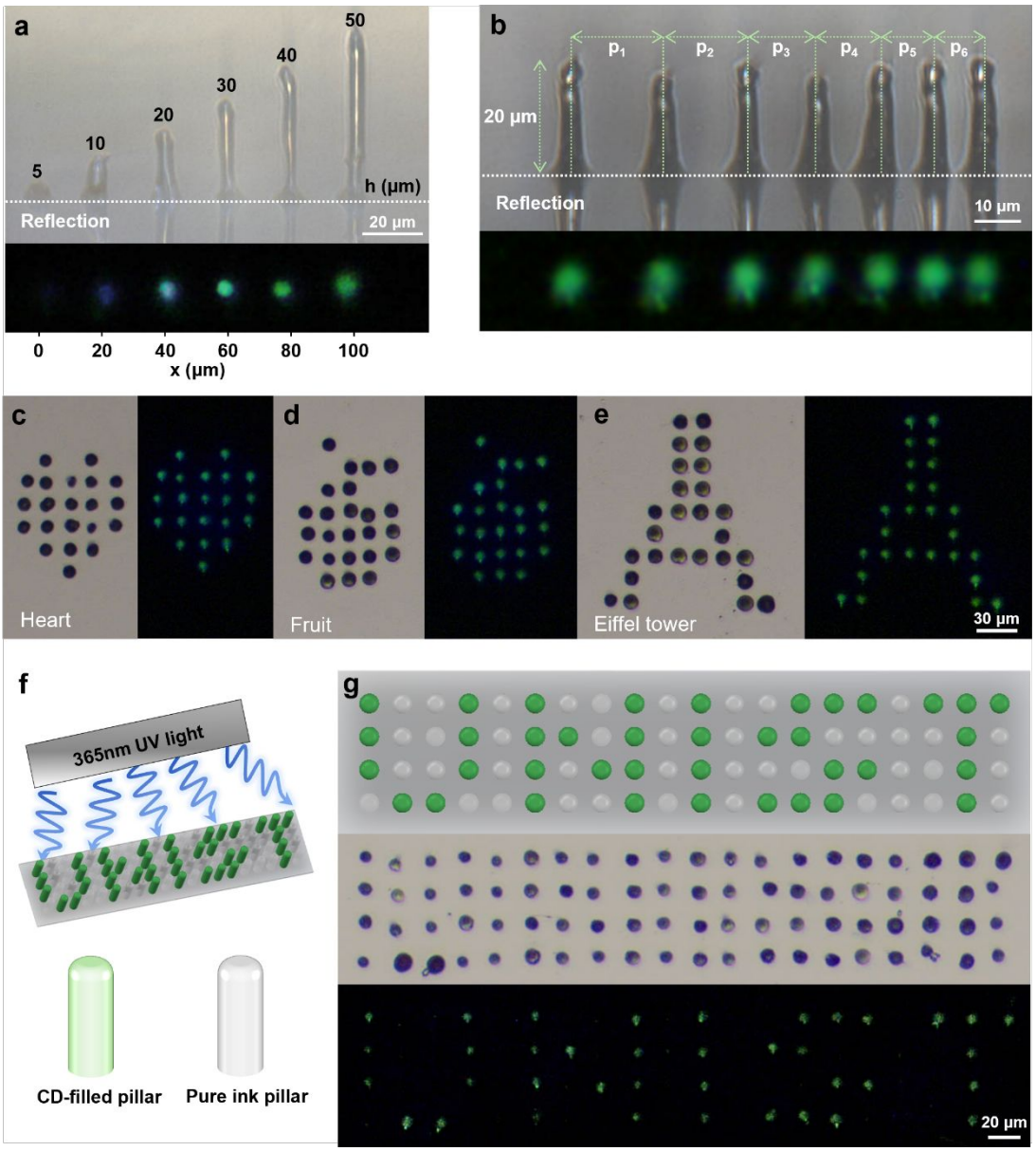


**Fig. 7.** Printing application using pillar structures. **a.** Side-view optical image comparing the brightness at different pillar heights. **b.** Optical side-view image of pillars arranged at varying intervals ($p_1$: 20 μm, $p_2$: 17.5 μm, $p_3$: 15 μm, $p_4$: 12.5 μm, $p_5$: 11.25 μm, $p_6$: 10 μm). **c-e.** Fluorescence images of different patterns **c.** heart, **d.** fruit, **e.** Eiffel tower. **f.** Schematic of information encryption method using CD-filled pillars and pure ink pillars under 365nm UV light. **g.** Encrypted image of the text "UNIST".

Supporting Information

# Three-Dimensional Encrypted Printing of Carbon Dots via Meniscus-Guided Microprinting

Seobin Park[1,†], Sejeong Seo[3,†], Jae Eun Kim[1], Hyeonjin Park[3], Woosung Kwon[3,4]*, Im Doo Jung[1,2]*

[1]Department of Mechanical Engineering, Ulsan National Institute of Science and Technology (UNIST), Ulju-gun, Ulsan, 44919, Republic of Korea

[2]Artificial Intelligence Graduate School, Ulsan National Institute of Science and Technology (UNIST), Ulju-gun, Ulsan, 44919, Republic of Korea

[3]Department of Chemical and Biological Engineering, Sookmyung Women's University, 100 Cheongpa-ro 47-gil, Yongsan-gu, Seoul, 04310, Republic of Korea

[4]Institute of Advanced Materials and Systems, Sookmyung Women's University, 100 Cheongpa- ro 47-gil, Yongsan-gu, Seoul, 04310, Republic of Korea

†These authors equally contributed to this work

*Corresponding authors: Woosung Kwon, Im Doo Jung

E-mail: wkwon@sookmyung.ac.kr, idjung.unist.ac.kr

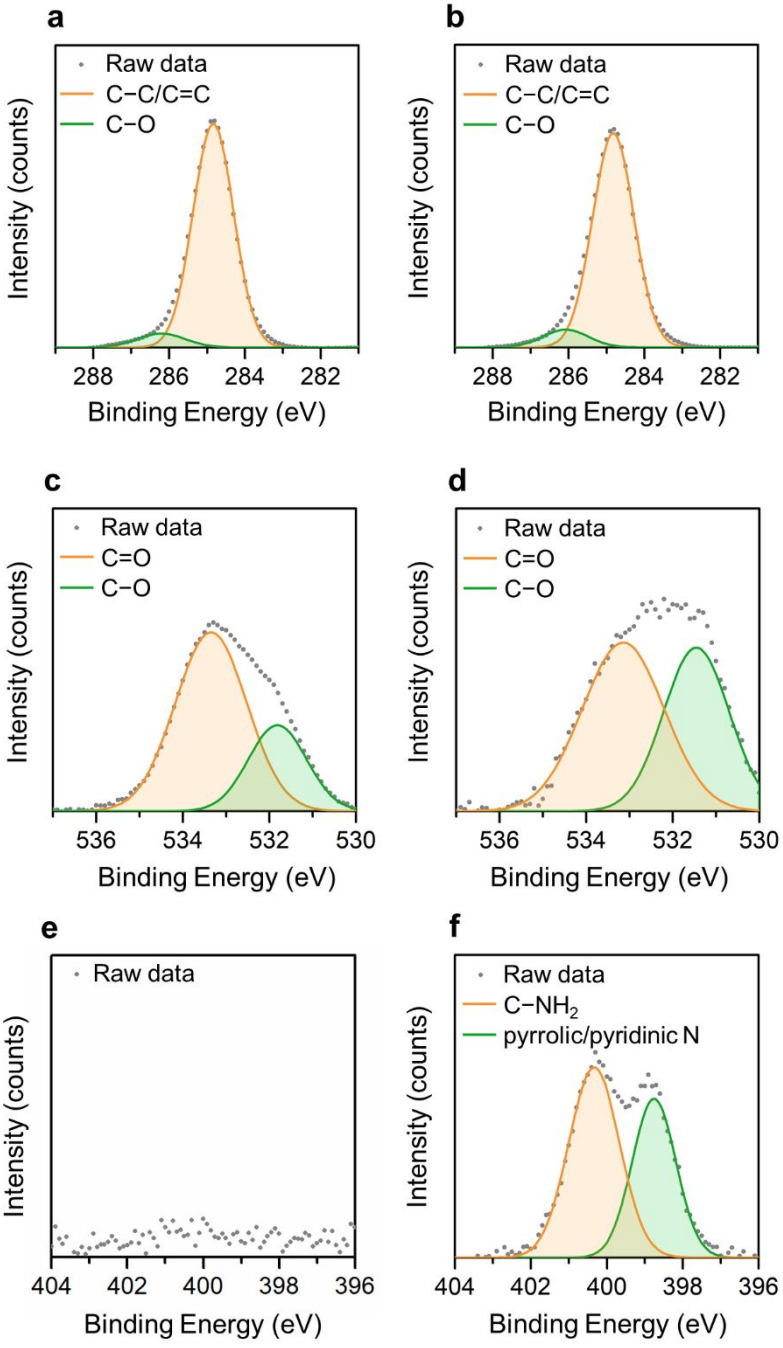


**Fig. S1.** High-resolution **a, b.** C 1s, **c, d.** N 1s, and **e, f.** O 1s XPS profiles of **a, c, e.** O-CDs and **b, d, f.** N-CDs.

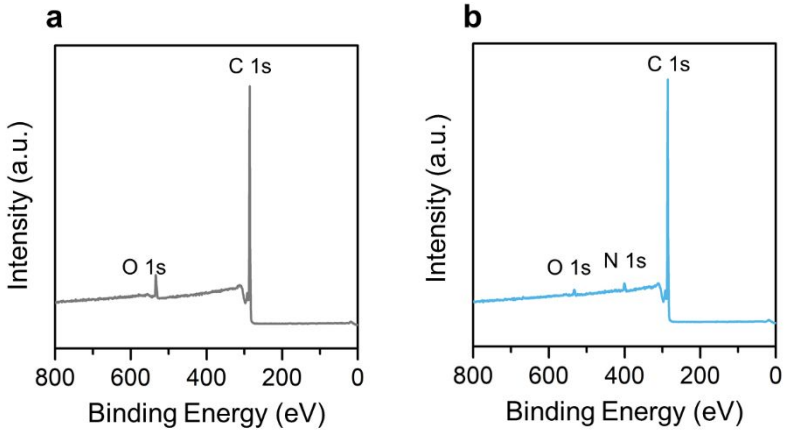


**Fig. S2.** XPS survey spectra of **a.** O-CDs and **b.** N-CDs.

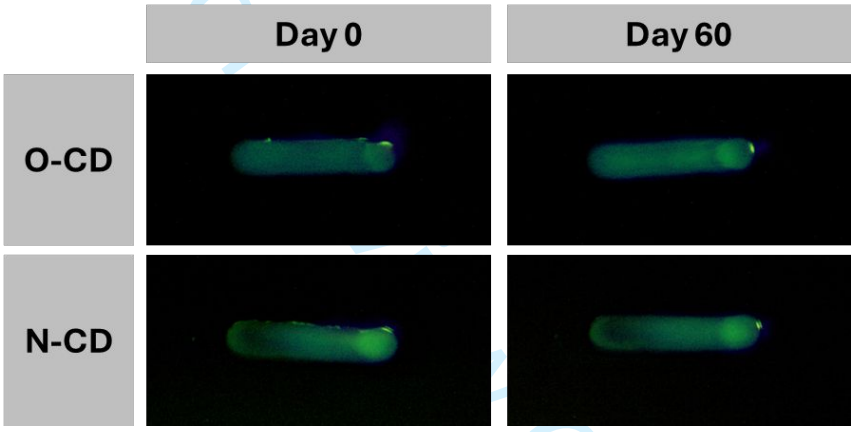


**Fig. S3.** The fluorescent stability test of the O and N-CDs filled printed lines at the room temperature for 60 days.

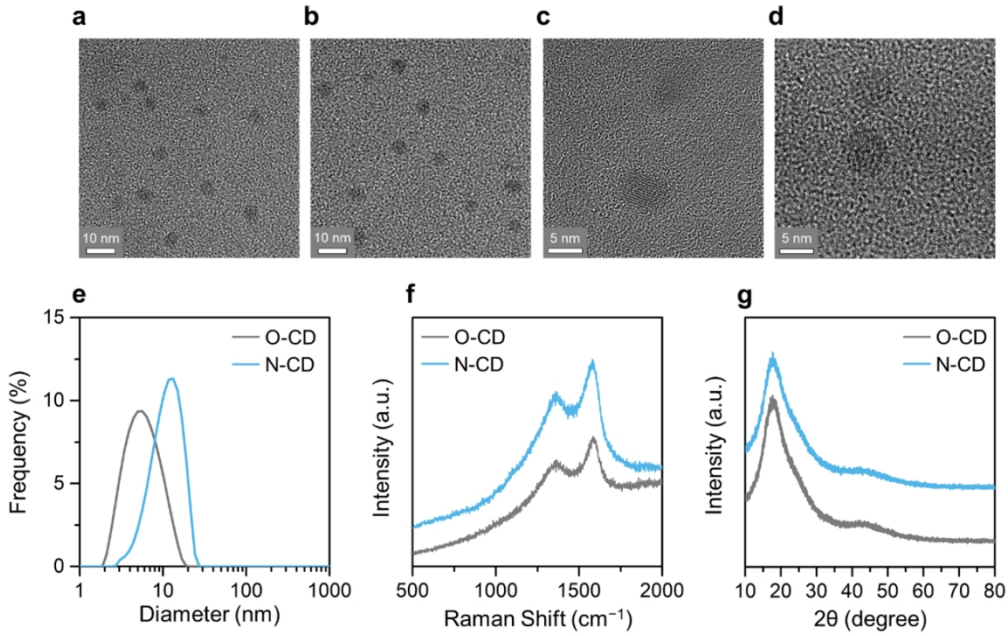


Fig. 1. Morphological characterizations of the CDs. TEM images of a. O-CD and b. N-CD. High-resolution TEM images of c. O-CD and d. N-CD. e. DLS size-distribution curves of the CDs. f. Raman spectra of the CDs. g. XRD patterns of the CDs.

146x92mm (220 x 220 DPI)

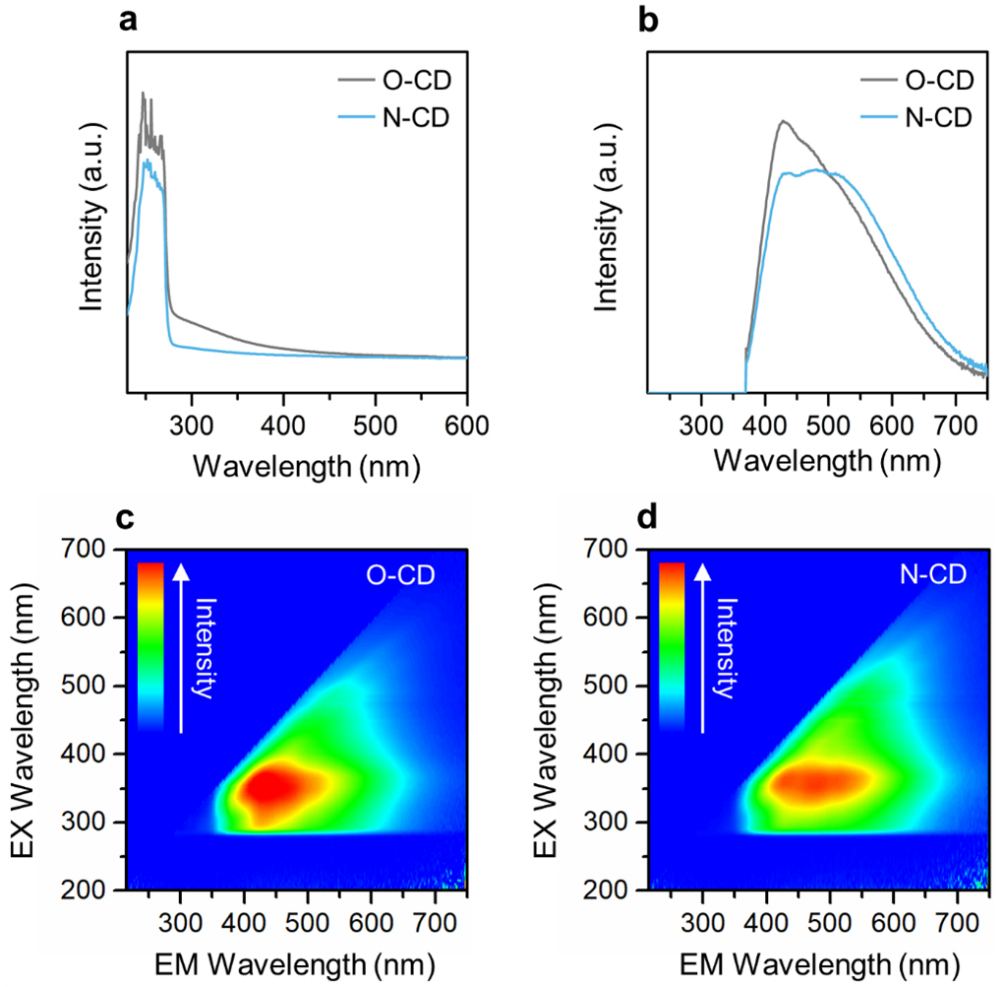


Fig. 2. Optical analyses of the CDs. a. ABS spectra of the CDs. b. PL emission spectra of the CDs. PL emission contour maps of c. O-CD and d. N-CD. EX and EM in the axis titles refer to excitation and emission, respectively.

117x115mm (220 x 220 DPI)

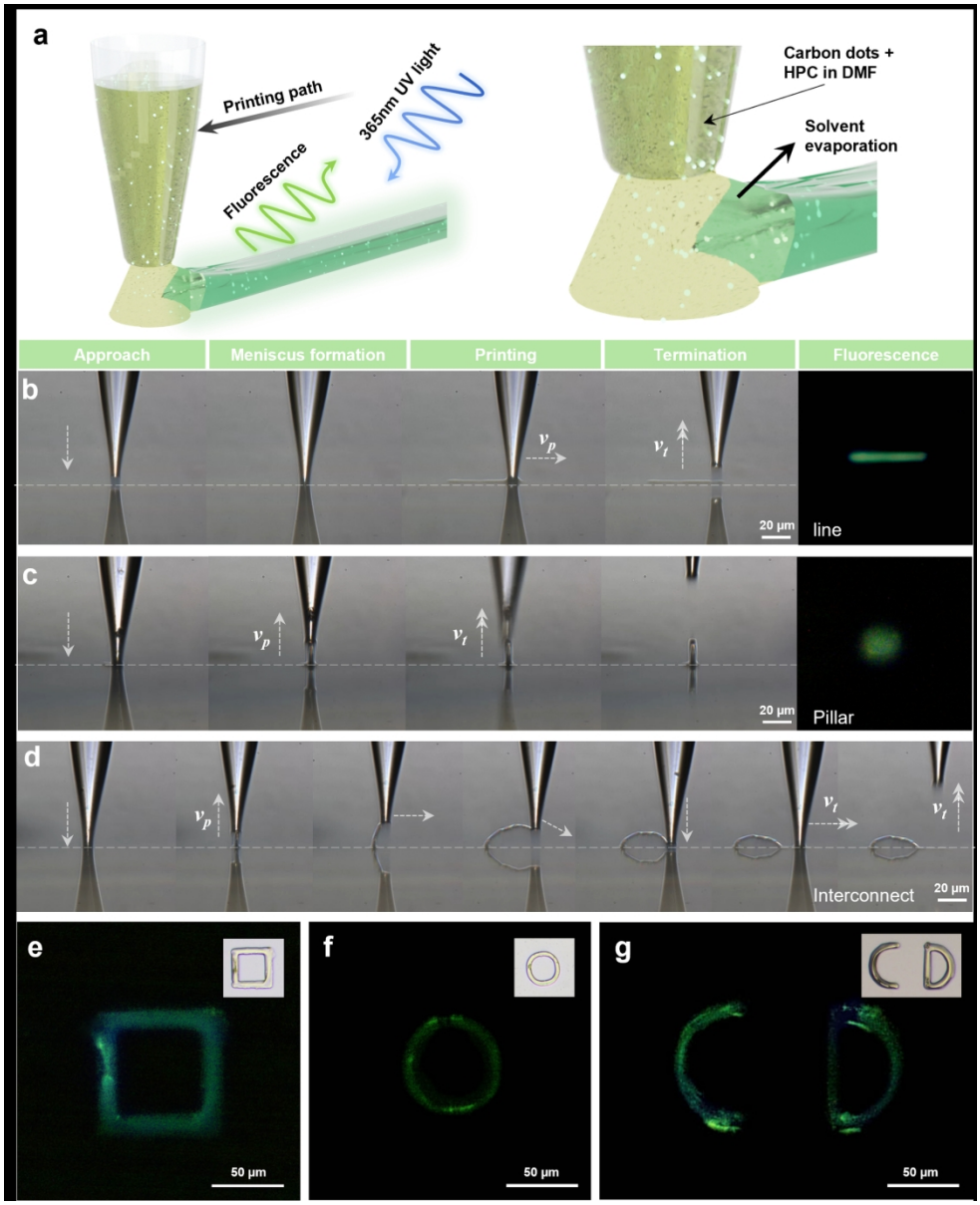


Fig. 3. Meniscus-guided micro printing of the CD-filled ink and printing techniques. a. Schematic of printing and fluorescence in printed patterns under UV light. b-d. Various printing techniques for printing of b. line, c. pillar, d. interconnect and their fluorescence images. e-g. Printing applications for writing a plane figures and alphabets using continuous layer-by-layer printing method.

167x206mm (300 x 300 DPI)

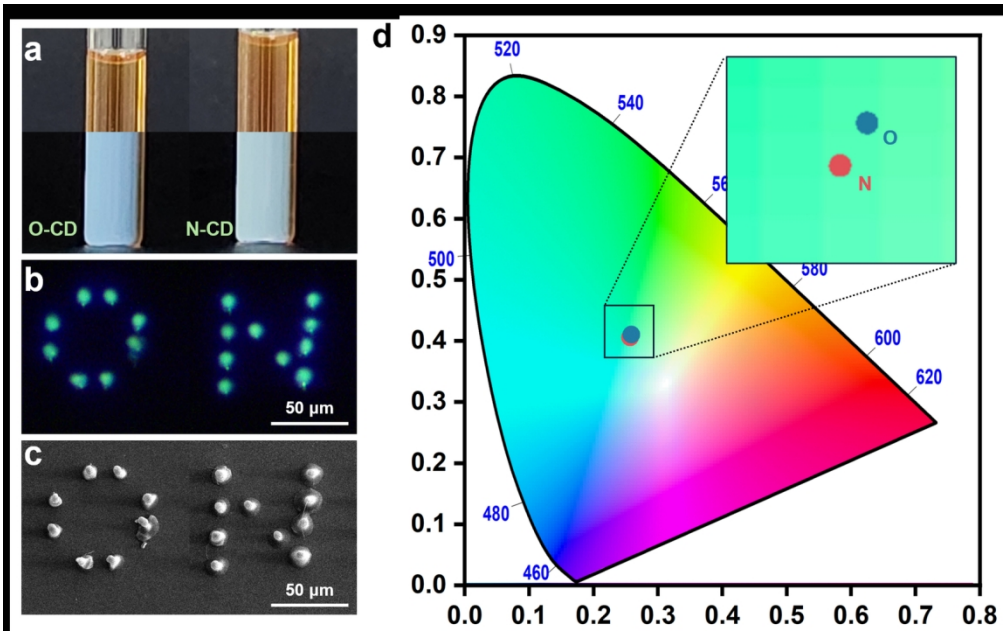


Fig. 4. a. Optical images of the O- and N-CD-filled inks under daylight and 365 nm UV light. b. Optical images of the printed CD ink and comparison of fluorescence colors of the pillars filled with O- and N-CD. c. SEM image of the letter "O" and "N". d. CIE chromaticity diagram of color coordinates of O- and N-CD fluorescence colors.

146x91mm (300 x 300 DPI)

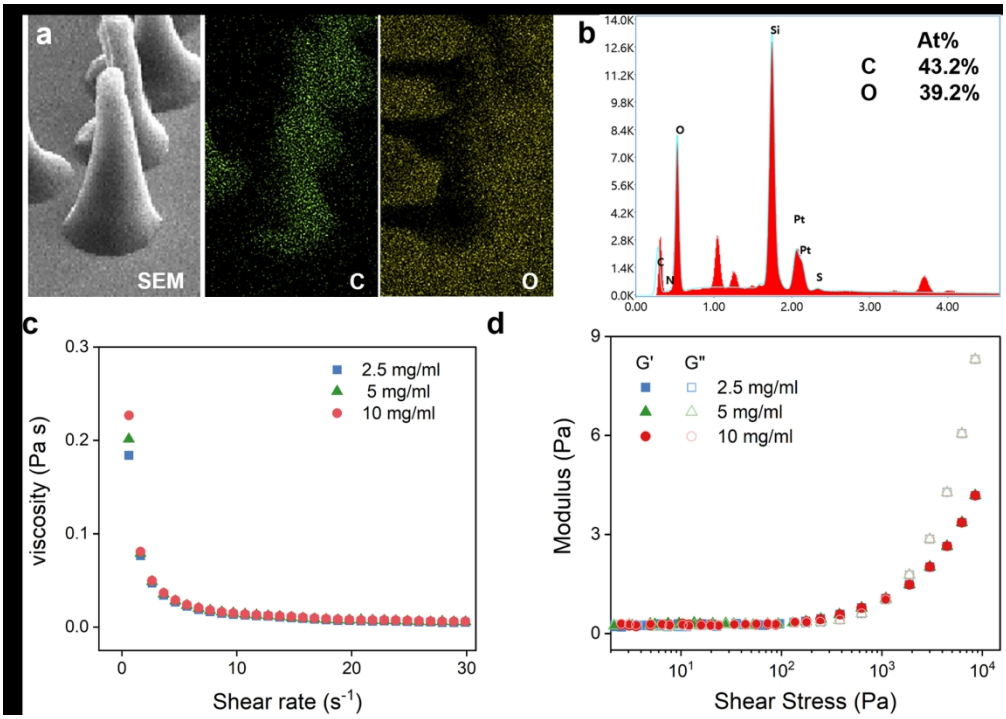


Fig. 5. a. EDS images of the elemental mapping in the printed structures. b. energy spectrum results of CD-HPC architectures. c, d. Rheological properties of CD-HPC inks with different HPC concentration.

161x115mm (300 x 300 DPI)

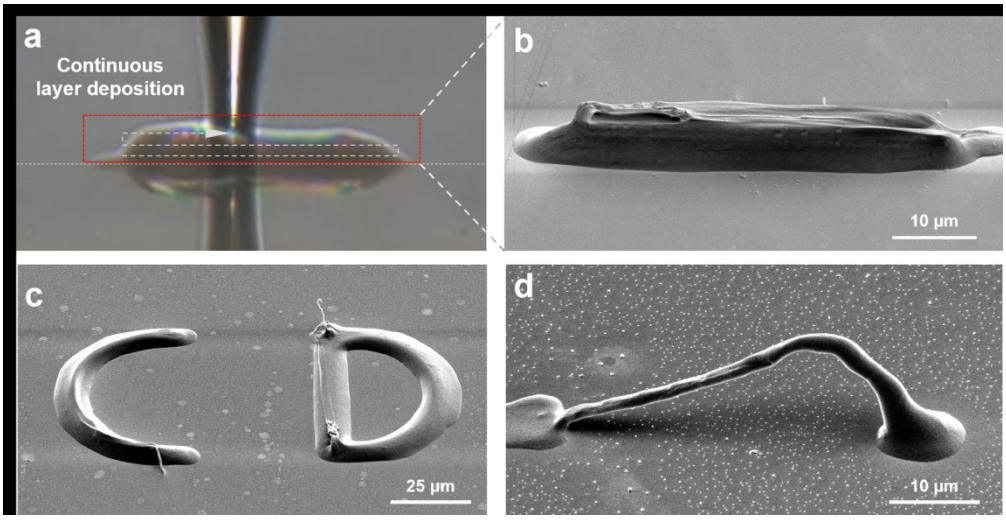


Fig. 6. Optical and SEM images of different printed structures. a, b. wall structure printed through continuous layer deposition, c. letter "CD" with multi-layer printing, d. Single-arch interconnect structure.

145x74mm (300 x 300 DPI)

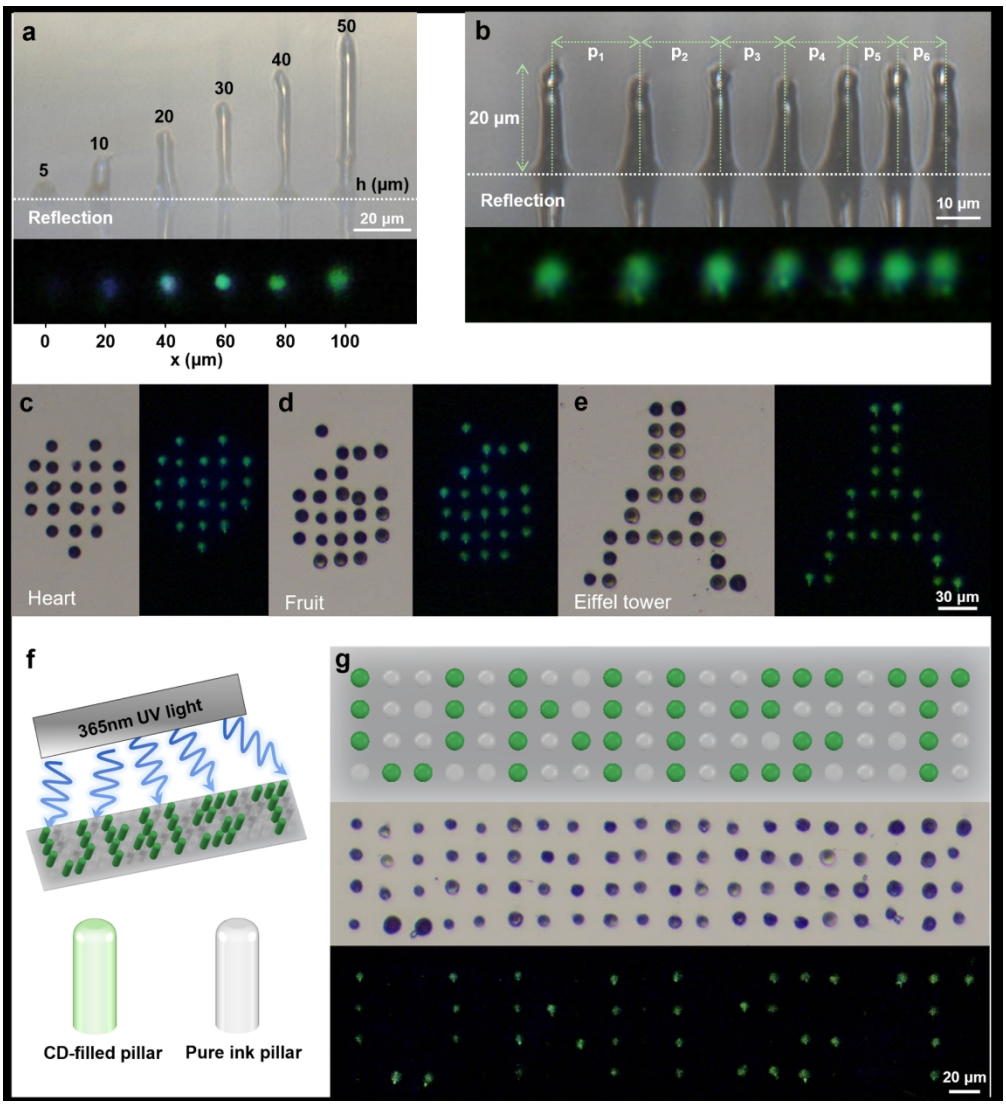


Fig. 7. Printing application using pillar structures. a. Side-view optical image comparing the brightness at different pillar heights. b. Optical side-view image of pillars arranged at varying intervals (p1: 20 μm, p2: 17.5 μm, p3: 15 μm, p4: 12.5 μm, p5: 11.25 μm, p6: 10 μm). c-e. Fluorescence images of different patterns c. heart, d. fruit, e. Eiffel tower. f. Schematic of information encryption method using CD-filled pillars and pure ink pillars under 365nm UV light. g. Encrypted image of the text "UNIST".

161x176mm (300 x 300 DPI)

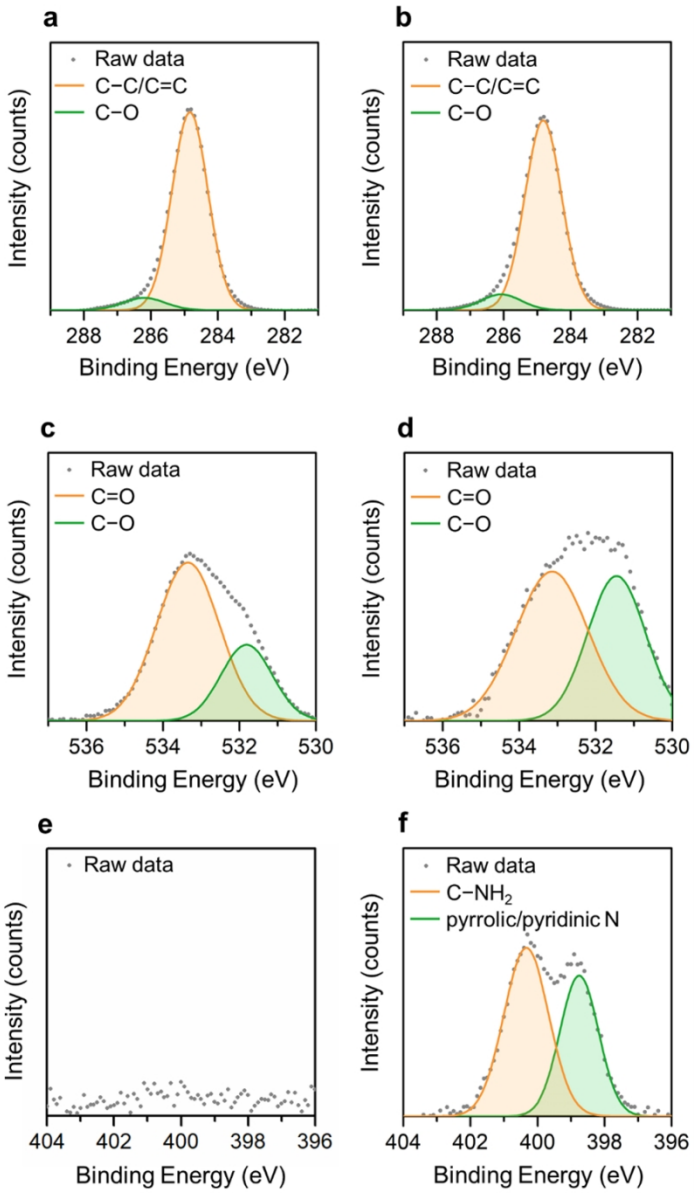


Fig. S1. High-resolution a, b. C 1s, c, d. N 1s, and e, f. O 1s XPS profiles of a, c, e. O-CDs and b, d, f. N-CDs.

104x179mm (220 x 220 DPI)

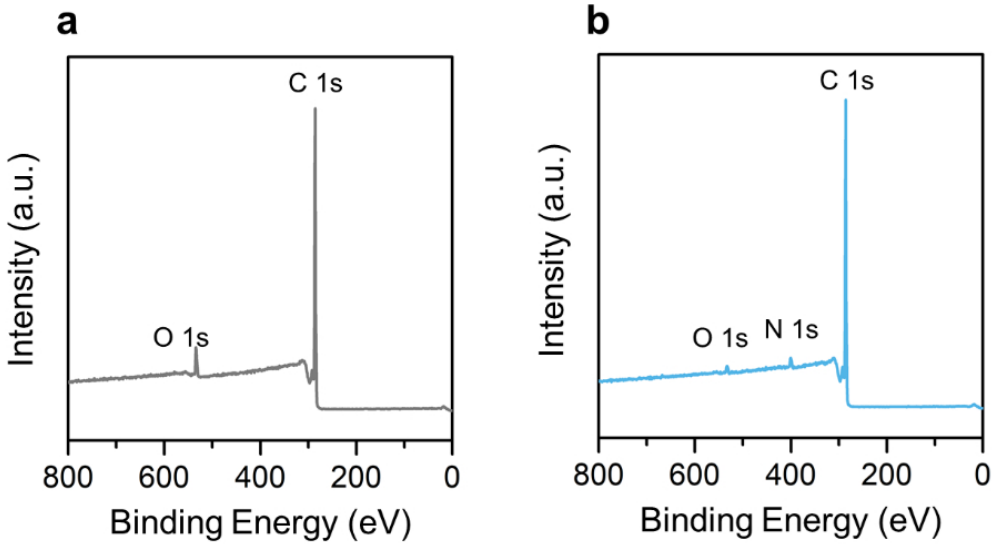


Fig. S2. XPS survey spectra of a. O-CDs and b. N-CDs.

104x57mm (220 x 220 DPI)

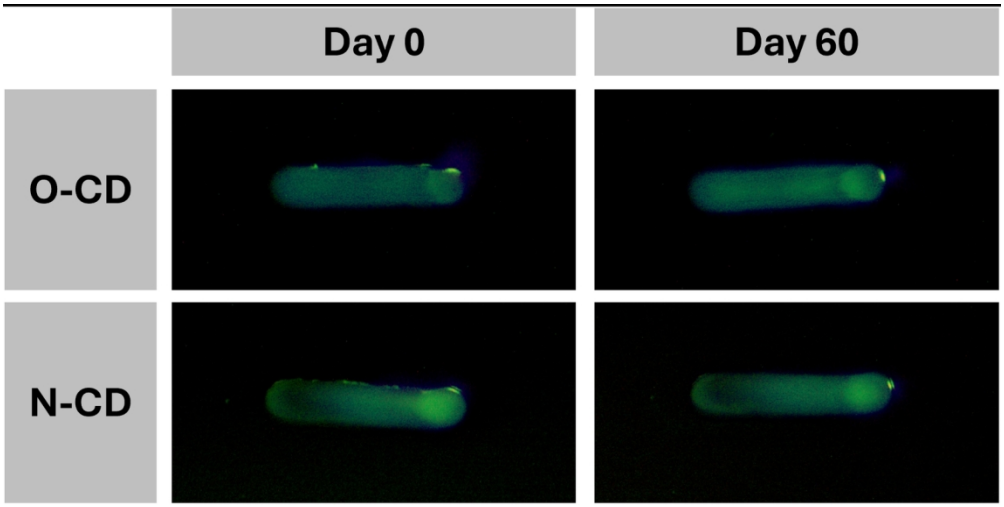


Fig. S3. The fluorescent stability test of the O and N-CDs filled printed lines at the room temperature for 60 days.

151x75mm (300 x 300 DPI)